Cranfield

College of Aeronautics Report No. 8421
May 1984

Some Effects of Sweep Direction and Strakes for Wings with Sharp Leading Edges

by D.I.A. Poll and Cheng-Hao Qiu

College of Aeronautics
Cranfield Institute of Technology
Cranfield, Bedford MK43 0AL
England

Peking Institute of Aeronautics and Astronautics
Peking, China

Cranfield
College of Aeronautics Report No. 8421
May 1984

Some Effects of Sweep Direction and Strakes for Wings with Sharp Leading Edges

by D.I.A. Poll and Cheng-Hao Qiu

College of Aeronautics
Cranfield Institute of Technology
Cranfield, Bedford MK43 0AL
England

Peking Institute of Aeronautics and Astronautics
Peking, China

ISBN 0 947767 088

£7.50

Summary

An experimental investigation has been carried out to compare the effects of sweep direction upon the aerodynamic characteristics of three wing planforms, each with sharp leading edges. The wings have biconvex aerofoil sections which allow them to be tested in both the forward-swept and backward-swept configurations without changing the section profile. Measurements of lift, drag and pitching moment have been made for angles of incidence in the range -5^{o} to $+50^{o}$ at a mean chord Reynolds number of approximately 1.5×10^{5} and a Mach number of 0.1. To complement the force and moment data a comprehensive series of oil-flow visualisations are also presented. In addition the aerodynamic characteristics of simple strakes (wing root fillets) have been studied for both the swept-forward and swept-back configurations.

Introduction

Historically, sweep was applied to wings in order to delay the drag rise Mach number and, hence, improve the aerodynamic performance in the transonic speed range. The direction of this sweep, i.e. forward or backward, has usually been determined by structural considerations. Simply stated, the ultimate performance of a wing is limited by the onset of an instability resulting from a coupling of the aerodynamic loading and the attendant elastic distortion of the structure. This instability maybe either torsional divergence or bending/torsion flutter - see Bisplinghoff et al[1]. For a given wing each of these phenomena arise as a critical speed is exceeded and, in general, these speeds are strongly dependent upon both the magnitude of the sweep angle and its direction. In the case of the swept-back wing the flutter speed is usually encountered first but the critical speeds for both divergence and flutter increase with increasing sweep angle. However, when the wing is swept forward the critical speed for the divergence drops very rapidly and this becomes the dominant instability at all but the smallest sweep angles. For this reason metal wings with forward sweep have always turned out to be prohibitively heavy compared to swept-back wings. Consequently, with one or two notable (and unsuccessful) exceptions, high speed aircraft have always had swept-back wings. This, in turn, has meant that virtually all the applied aerodynamic research conducted up to the present time has been directed towards an improved understanding of the flows over swept-back wings. Recently, developments in composite material technology, have removed this traditional obstacle to forward sweep since it is now possible to tailor structural behaviour so that the divergence problem is suppressed without incurring a weight penalty - see Krone[2]. Therefore, there is currently considerable interest in the aerodynamic performance of swept forward wings.

The primary aim of the present work was to conduct a simple experiment which would demonstrate the effects of sweep direction on the aerodynamic characteristics of several wing planforms with sharp leading edges as indicated by the variation of lift, drag

and pitching moment with incidence. In order to reduce the number of independent variables to the minimum each of the wings tested had simple uncambered bi-convex aerofoil sections and the planforms were untwisted. Consequently, direct comparisons are possible, since each wing could be mounted in either a forward or backward swept configuration whilst aspect ratio, taper ratio, geometric incidence and aerofoil section remained unchanged. To compliment the force and moment measurements and also obtain a more complete qualitative understanding of the phenomena involved, a comprehensive series of surface oil-flow visualisations have been produced. In addition, whilst it is well known (e.g. Lamar and Frink[3]) that the performance of swept-back wings at high incidence may be dramatically improved by the addition of strakes, it is not at all clear whether strakes will improve the performance of forward swept wings. Doubts arise because in the former case the strake vortex has the same sense of rotation as the wing vortex and, consequently, tends to enhance its lifting characteristics. In the latter case, however, the strake and wing vortices have opposite senses of rotation and this may result in reduced performance. To shed some light on this issue the effect of main wing sweep direction on strake/wing performance has also been investigated.

Finally, since the wings considered here have sharp leading edges, which effectively fix the location of boundary layer separation at all but the smallest incidences, it is unlikely that the results would exhibit strong Reynolds number dependence. However, it must not be assumed that the present findings are representative, or indicative, of the behaviour of wings with rounded leading edges at any Reynolds number, or of any wings with cambered aerofoil sections and/or spanwise twist distributions. Rather, it is intended that these results should form a very simple base-line against which future test data may be compared.

1. The Models and Test Conditions

The planforms of the wings chosen for the test programme are shown in figures 1 and 2, leading particulars are summarised in table 1. Each of the strakes shown in the figures has a wedge section in both the chordwise and spanwise direction i.e. their leading edges are all sharp. In all cases the leading edge sweep is greater than 70° and so the vortices which they produce are stable and strong. With the exception of S3-B (curved leading edge) the strakes are sized so that the chord, the ratio of strake area to wing area and the ratio of strake to wing semi-span are the same in both the swept-forward and the swept-back configuration. The standard body, which supports each wing during the test, consists of an ogive nose ($\ell/d = 2$) and a cylindrical body ($\ell/d = 10$).

The tests were carried out in a closed return circuit wind-tunnel with an open jet working section of eliptic cross-section (1 m x 0.7 m). Forces and moments were measured using a three-component wind-tunnel balance situated beneath the jet. All the measurements and the oil-flow visualisations were performed at a wind speed of 30 m/sec, giving a Reynolds number based upon the mean aerodynamic chord of the wings of between 1.2×10^5 and 1.8×10^5. The aerodynamic coefficients were based upon the reference areas and reference lengths listed in table 1. Pitching moments were referred to the ¼ mean aerodynamic chord position of each configuration - the distance of this point from the apex of the standard body is also given in table 1. Since the dimensions of the models are small relative to those of the tunnel no attempt has been made to correct the results for the effects of blockage or lift interference.

2. Characteristics of the Basic Wings

For untwisted wing planforms with symmetrical aerofoil sections linearised potential flow theory suggests that the lift-curve slope and induced drag coefficients are the same for both swept-forward and swept-back configurations. This result is embodied in the reverse flow theorem[4]. Since the aerofoil section used here is the same whether the sweep is forward or backward, any dependence of sweep sign in the aerodynamic characteristics at small angles of incidence is probably the result of wing/body interference and the different three-dimensional effects within the boundary layers. In addition, because the wings have sharp leading edges, there may also be changes due to the loss of leading edge suction. However, the principal differences between the swept-forward and swept-back configurations are expected to occur at high incidences where the aerodynamic characteristics are determined by the non-linear behaviour of the separated vortex flows.

a) Planform W2

The results of the force and moment measurements for planform W2 are presented in figure 3. It can be seen from the C_L versus α plot that in the forward sweep case (W2 - F) a linear behaviour is obtained up to an incidence of 9^o. Beyond this point the lift continues to increase with incidence at a progressively slower rate until the maximum lift coefficient of 1.15 is reached at an incidence of 35^o. A similar trend is found for the backward swept case (W2 - B) where the linear lift-curve slope extends to 13^o and a maximum lift coefficient of 1.12 occurs at approximately 40^o. Both configurations have almost the same lift-curve slope at low incidence. It should be noted, however, that between 18^o and 39^o the lift is greater in the forward sweep case. The C_D versus C_L plot shows that below a lift coefficient of 0.5 ($\alpha<9^o$) the total drag coefficients do not depend upon sweep direction. For C_L lying between 0.5 and 0.84 the swept forward wing has a higher drag for a given lift, with maximum difference being approximately 15% at a lift coefficient of 0.63. In this same C_L range the swept back wing produces slightly more lift at a fixed angle of incidence. Beyond a C_L of 0.84 the swept forward wing has less drag for a given lift.

Variations of pitching moment with lift clearly indicate the presence of several distinct regimes for each configuration. For the swept-forward case dC_M/dC_L is negative for lift coefficients below 0.6 ($\alpha<10^o$). Between a C_L of 0.6 and 1.1 dC_M/dC_L is positive and almost constant. Beyond a C_L of 1.1 there is a rapid increase in C_M as incidence is increased through 35^o. When the wing is swept-back dC_M/dC_L is positive and small for lift coefficients below 0.7 ($\alpha<13^o$). For lift coefficients between 0.7 and 1.15 dC_M/dC_L is much larger but still approximately constant and roughly equal to dC_M/dC_L for the swept-forward wing over the same range of lift coefficient. There is no rapid pitch up tendency in the vicinity of $C_{L_{max}}$ for the swept-back case. Finally, the plot of L/D versus C_L shows that the maximum lift to drag ratio occurs at the uppermost end of the linear lift-curve slope region ($\alpha\simeq10^o$) and, consequently, it is approximately independent of sweep direction. At lift coefficients between 0.40 and 0.84 the swept-back wing has better L/D characteristics, but beyond a C_L of 0.84 the L/D of the swept-forward wing is superior.

Surface oil-flow patterns for W2-F and W2-B for incidences in the range -5^o to $+50^o$ are presented in plate 1. For angles below 5^o both configurations exhibit the long bubble behaviour typical of aerofoils with small leading edge radii. As the incidence increases the bubble structure breaks down and a strong leading edge vortex is formed with its origin at the upstream apex (tip for W2-F, root for W2-B). The characteristic attachment and secondary separation lines are clearly visible in both configurations - see for example the patterns at 10^o. The visualisations indicate that for the swept-forward wing the bursting reaches the trailing edge at an incidence of about 9^o whilst in the backward-swept case bursting reaches the trailing edge at an incidence of roughly 12^o. This is consistent with the departure from linearity in the lift curve slope and the sudden change in the value of dC_M/dC_L. The variations of vortex orientation and the burst location for incidences beyond 10^o are summarised in figure 4. For incidences lying between 10^o and 17.5^o there are significant differences in the results for the two cases. When the wing is swept back the vortex makes a constant angle of approximately 18^o with the leading edge, whilst the burst moves progressively towards the root apex as incidence is increase. However, when the wing is swept forward, the angle

between the vortex and the leading edge increases from 9° at an incidence of 10° to 16° at an incidence of 17.5°. At the same time the burst moves towards the tip apex but the distance from the apex to the burst, as measured along the vortex path, is always greater than that observed for the swept back configuration. It should be noted that, for this particular incidence range, the results presented in figure 3 indicate that the wing with backward sweep has the better characteristics. At incidences above 17.5° the vortex orientations are very similar for both cases but the vortex burst is always closer to the apex when the wing is swept-back. This delaying of the vortex burst accounts for the improved performance of the swept forward wing at incidences between 18° and 39° (see figure 3). Beyond the maximum lift condition the flow in both cases became very unsteady and this behaviour is apparent from the lack of definition in the oil-flow patterns at the largest incidences.

The visualisations also give a clear indication that the forward swept wing is likely to have a larger maximum usable lift coefficient. Figure 5 shows the loading distributions for this planform as predicted by linearised potential flow theory[5]. The maximum loading occurs at the root for the swept-forward wing and at about 60% of the span for the swept-back case. This suggests that the former will have a stall which begins in the root and the latter will have a stall which beings in a region out towards the tip. The results presented in plate 1 confirm that the stalls do develop in precisely this way. Since roll control devices are likely to be located close to the wing tips they will loose their effectiveness at relatively low incidence in the swept-back case. However, if the wing has forward sweep, control effectiveness will be maintained to a very high incidence by the flow induced by the powerful leading edge vortex - see plate 1 and figure 4.

b) Planform W1

The force measurements for this wing are presented in figure 6 and the surface oil-flow patterns are presented in plate 2. As in the previous case, the lift and drag characteristics at low incidence are approximately independent of sweep direction. For the swept-back configuration (W1 - B) the behaviour at angles of incidence greater than 5° is very similar to that observed for planform W2 - B. The departure from linearity in the lift-curve slope and a discontinuity in dC_M/dC_L coincide with the appearance of a vortex burst at the trailing edge ($\alpha \simeq 8^{\circ}$). As the incidence increases the burst moves towards the vortex origin at the wing root apex maintaining an almost constant value of dC_M/dC_L up to the largest incidence. The maximum lift coefficient achieved is 1.0 and this occurs at an incidence of approximately 35°. The behaviour of the swept-forward configuration is different from that observed for W2 - F. In this case the oil-flow shows that the leading edge vortex does not turn downstream as the root is approached. Instead a burst occurs in the root close to the leading edge. This feature is clearly visible at 5° of incidence. As the angle of attack is increased the burst point moves along the leading edge towards the tip and so there is no situation in which the burst crosses the trailing edge of the wing. This is clearly demonstrated on the plot of C_M versus C_L where it can be seen that there is no discontinuity of dC_M/dC_L. Furthermore the burst is very close to the tip apex at an incidence of about 20° as opposed to 30° for W2 - F. At incidences above 20° the oil-flow patterns are all very similar, the lift generated by the wing is almost independent of α but the centre of pressure moves forward rapidly producing a sharp pitch up behaviour. The drag at high incidence for the swept-forward planform is very much higher than for the swept-back planform for the same lift coefficient. Therefore at high incidence the backward-swept configuration has a much better lift to drag ratio. The maximum lift to drag ratio, however, occurs in the range of the linear lift-curve slope and, therefore, it is independent of sweep direction.

At high incidences the characteristics of the forward and backward swept configurations of planform W1 show much larger differences than was the case for planform W2 (figure 3). This is because the flow behaviour is governed by the vortex which is fed by the boundary layer separation at the sharp leading edge and, clearly, the leading edge sweep angle will have a powerful influence on the properties of this vortex. In the case of planform W2 the leading edge sweep was unaffected by a change in the sweep direction. However, since planform W1 has taper ($\lambda = 0.287$), it follows that a reversal of the sweep direction is necessarily accompanied by a change in the sweep angles of both the leading end trailing edges. Therefore in the backward swept case (W1 - B) the leading edge sweep is 40° whilst in the forward swept case (W1 - F) it is only 20°. Previous experience with untwisted aerofoils with sharp, swept leading edges indicates that for sweep angles between 15° and 30° a weak type of spiral vortex flow is established - see for example Poll[6]. Therefore the relatively poor performance of W1 - F is due, primarily, to the low leading edge sweep angle. In addition it was previously noted that W1 - B and W2 - B exhibit very similar behaviour. This is to be expected since the leading edge sweep angles differ by only 5° and both sweeps are sufficiently large for the development of a strong vortex flow.

c) Planform W3

The experimental results for planform W3 are given in figure 7 and plate 3. For the forward-swept configuration the results are very similar to those obtained for planform W1 - F. Departure from the linear lift-curve slope occurs at a C_L of about 0.6 with the maximum C_L (0.86) being reached at an incidence of 38°. The plot of C_M versus C_L shows no discontinuity of slope in the incidence range below 38° and the pitch-up tendency in the vicinity of $C_{L_{max}}$ is less marked than in the previous cases. Oil-flow patterns confirm that the vortex burst phenomena always occurs over the wing itself. The development of the oil-flow pattern with incidence is much the same as that observed on W1 - F (plate 2). As in the previous case the overall similarity between the results for W3 - F and W1 - F is attributable to the leading edge sweep angles. WF - 3 has a leading edge sweep of 30° whilst for W1 - F it is 20°. Both these angles are sufficiently

small for the formation of the weak spiral vortex flow. When the wing is reversed the lift and drag variations are very similar to the forward swept values for angles below 5^{o}. Above 5^{o} the strong leading edge vortex, which is clearly visible in the oil-flow patterns, continues to produce lift to such a degree that the $C_L - \alpha$ curve is approximately linear up to an incidence of 18^{o}, whilst improved drag performance is evident at incidences beyond 12^{o}. The maximum lift coefficient for this case is 1.16 and this occurs at an incidence of 32^{o}. The pitching moment against lift coefficient plot shows that a vortex burst reaches the trailing edge at an incidence of about 15^{o}. This incidence is somewhat higher than the values observed for the other swept-back planforms but the trend towards higher incidence as wing sweepback is increased is consistent with the general behaviour of slender delta wings - see Küchemann[7]. The oil-flow patterns show that at incidences beyond 15^{o} the secondary separation line lies close to the leading edge and, therefore, the vortex core follows a line joinging the root apex to the mid-point of the trailing edge. The low pressures induced on the surface by the vortex act over a large area and, consequently, a high maximum lift coefficient is obtained. However, in spite of the differences in the leading edge vortex flows, the maximum lift to drag ratio is, once again, essentially independent of sweep direction.

3. The Effects of Strakes

The results for the straked configurations shown in figures 1 and 2 are presented in figures 8, 9 and 10. By comparing these results with those given in figures 6,3 and 7 it is possible to assess the effectiveness of the strakes for the various configurations. At low incidence the lift curve slopes of all the wings are increased by between 5% and 14%. This is mainly due to the fact that whilst the straked wings have a greater lifting surface area than the basic wings, the references areas used to reduce the data to coefficient form were not changed when the strakes were added. In all cases the percentage improvements in the lift-curve slopes were less than the percentage increases in the surface area. At large incidences a general increase in the extent of the linear lift-curve slope region was observed along with corresponding increases in the values of the maximum lift coefficients. A general improvement is also apparent in the plots of drag coefficient against lift coefficient where drag is reduced at the higher lift conditions and the region in which drag is effectively independent of sweep direction is also extended. These benefits are offset to some extent by the positive dC_M/dC_L behaviour with a strong pitch up tendency in the vicinity of the maximum C_L in all cases. The overall improvements in lift coefficient are summarised in figure 11. Here it is of interest to note that at angles of incidence below 12^o the swept-forward configurations receive more benefit from the strakes. Between 12^o and 45^o ΔC_L is a complex function of the planform parameters. For W1 and W2 the strakes produce the largest improvements when the wings are swept-back, whilst for W3 the swept forward case is best. This latter result may, however, be due to the fact that the span of the strake is slightly larger for the forward swept configuration and, consequently, the strake vortex may influence a larger portion of the wing surface. The variation of lift to drag ratio with lift coefficient is plotted in figure 12. It is apparent that below the maximum value of L/D the strakes and the direction of the sweep has very little influence. Beyond $(L/D)_{max}$ the strakes improve the lift/drag ratio for all configurations, with the best performance being obtained on the swept-back planforms.

The oil-flow visualisations for the straked wings are presented in plates 4 and 5. For the swept-forward configurations at incidences below about 10° the wing may be viewed as two panels separated by an extension of the strake leading edge. Between this imaginary line and the fuselage side the flow pattern is similar to that found on a conventional slender delta with clearly defined primary attachment and secondary separation lines. On the other side of the line the flow patterns are very similar to those obtained on the unstraked wing. At incidences beyond 10° the planforms with the larger leading edge sweep angles (W2 - FS and W3 - FS) develop an extra separation line on the main wing. This is approximately parallel to, but displaced outboard from, the strake induced separation line. As incidence is increased these lines move closer together and ultimately give way to a single 'eye' structure which forms in the vicinity of the strake/wing junction. The 'eye' occupies this position until incidences of about 40° are reached. Beyond 40° the 'eye' moves towards the trailing edge and ultimately disappears. For the wing with the lowest leading edge sweep (W1 - FS) the 'eye' forms before the extra separation line can be established but its subsequent development with incidence is similar to that observed for W2 - FS and W3 - FS.

For the swept-back configurations oil-flow patterns have been obtained for planforms W1 - BS and W3 -BS. As in the swept-forward case at the lower incidences the wing may be divided into two panels by extending the strake leading edge across the main wing. The inner panel has the slender delta type of pattern whilst the outer panel has the general appearance of the unstraked wing. As incidence increases the secondary separation line on the outer panel is more clearly defined and reaches the trailing edge at a smaller incidence than was the case for the unstraked wing. Further increases in incidence result in a bursting of the strake vortex with the strake induced separation on the main wing gradually disappearing. At the highest incidences the secondary separation on the outer panel also disappears.

4. Conclusions

The investigation has shown that, in low-speed flow ($R_c \simeq 1.5 \times 10^5$, $M_\infty \simeq 0.1$), the aerodynamic characteristics of untwisted trapezoidal wing planforms having uncambered, biconvex aerofoil sections exhibit a dependence upon sweep direction which varies with incidence, sweep angle magnitude, taper ratio and aspect ratio.

At incidences below 10° the variation of lift and drag for the three planforms tested were virtually independent of sweep direction. When the incidence was greater than 10° the performance of the wings was largely determined by the behaviour of the shear layers which separated along the sharp leading edges. For leading edge sweep angles greater than 30° the shear layer rolls up to form a strong vortex which results in a good lifting performance. However, if the leading edge sweep is 30° or less, a weak vortex is produced and the lifting performance is relatively poor. Therefore a large sweep direction dependence is observed when the sweep angle magnitude, taper ratio and aspect ratio are such that the leading edge sweep is greater than 30° for the swept-back configuration but less than 30° for the swept-forward configuration. This was the case for planforms W1 and W3. In addition to the 'strong' or 'weak' nature of the leading edge vortex the sweep direction was also found to affect the orientation of the vortex and the location of vortex bursting. These effects were most noticeable on planform W2, which was untapered and where the forward swept wing had the better lifting performance for incidences between 18° and 39°. In all cases the swept forward wings had a more pronounced pitch up tendency in the vicinity of maximum C_L. The maximum lift to drag ratio however, always occured in the region of linear C_L versus α behaviour and was virtually independent of sweep direction.

The addition of strakes improved the lifting characteristics of all the configurations. For incidences below about 12° the forward swept cases obtained the largest improvement in lift coefficient. At higher incidences the degree of benefit depended upon sweep direction and the other planform parameters. In all cases the strakes produced a sharp pitch up tendency as the maximum lift coefficient was approached. The strakes produced only minor

changes in the maximum values of the lift to drag ratio. However, at the higher incidences, the strakes improved L/D for all configurations.

References

1. Bisplinghoff, R.L.
   Ashley, H.
   Halfman, R.L.
   Aeroelasticity.
   Addison-Wesley Publishing Company Inc., 1955

2. Krone, N.J.
   Divergence eliminated with advanced composites.
   AIAA Paper No. 75-1009, AIAA Aircraft Systems and Technology Meeting, Los Angeles, August 1975.

3. Lamar, J.E.
   Frink, N.T.
   Aerodynamic features of designed strake-wing configurations.
   AIAA Paper No. 81-1214, AIAA 14th Fluid and Plasma Dynamics Conference, Palo Alto, June 1981.

4. Heaslet, M.A.
   Lomax, H.
   General theory of high speed aerodynamics and jet propulsion. Volume IV.
   Oxford University Press, 1955.

5. Woodward, F.A.
   An improved method for the aerodynamic analysis of wing-body-tail configurations in subsonic and supersonic flow.
   NASA CR 2228, May 1973.

6. Poll, D.I.A.
   On the generation and subsequent development of spiral vortex flow over a swept-back wing. Paper No. 6, AGARD CP 342, Proceedings of the AGARD FDP symposium on the Aerodynamics of Vortical Type Flows in Three Dimensions, Rotterdam, Netherlands, April 1983.

7. Küchemann, D.
   The Aerodynamic Design of Aircraft.
   Pergamon Press, 1978.

WINGS	W1-F	W1-B	W2-F	W2-B	W3-F	W3-B
Sweep angles L.E. / T.E.	-20°/-40°	40°/20°	-45°/-45°	45°/45°	-30°/-60°	60°/30°
Sweep angles Mid-chord	-31°	31°	-45°	45°	-49°	49°
Aspect ratio	4.84		4.0		2.5	
Taper ratio	0.287		1.0		0.177	
Thickness / chord	0.08		0.05 (tip) - 0.10 (root)		0.06	
Body dia. / Wing span	10 %		12.5 %		15 %	
STRAKES	**S1-F**	**S1-B**	**S2-F**	**S2-B**	**S3-F**	**S3-B**
L.E. sweep angles	74°	78°	74°	79°	74°	80°
Exposed semi-span ratio (strake / wing)	17 %		15 %		33.5 %	29.4 %
Exposed area ratio (strake / wing)	13.1 %		14.3 %		29.4 %	
REFERENCE PARAMETERS	**W1-F and W1-FS**	**W1-B and W1-BS**	**W2-F and W2-FS**	**W2-B and W2-BS**	**W3-F and W3-FS**	**W3-B and W3-BS**
Reference area, mm^2 (the gross area of basic wing)	18600	18600	14400	14400	16000	16000
Reference length, mm (the mean aerodynamic chord of basic wing)	68.6	68.6	60	60	93.1	93.1
Reference point, mm (from nose of body to 0.25 of mean aerodynamic chord)	190	236	150	240	180	244

Table 1.

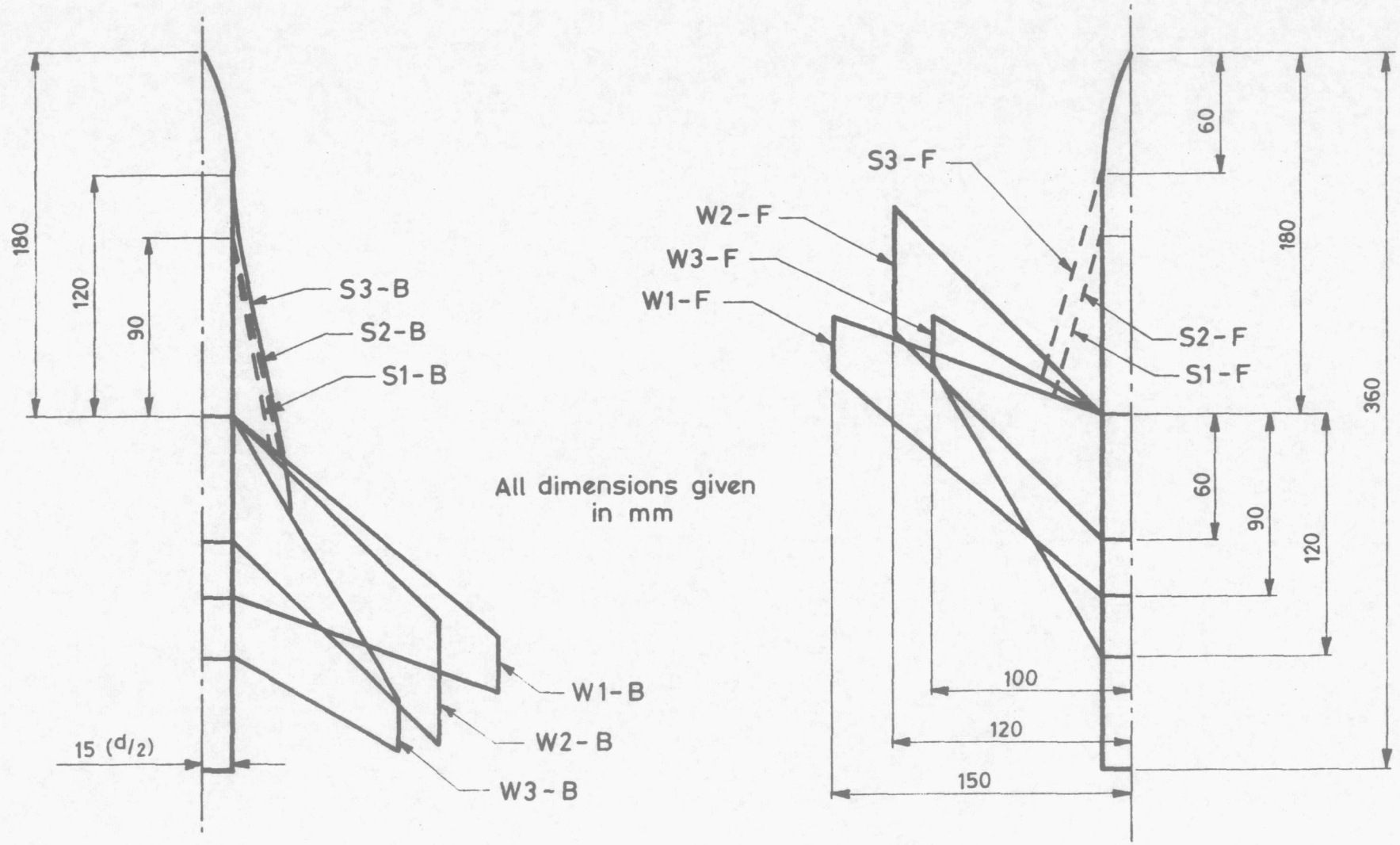

Figure 1. Model dimensions.

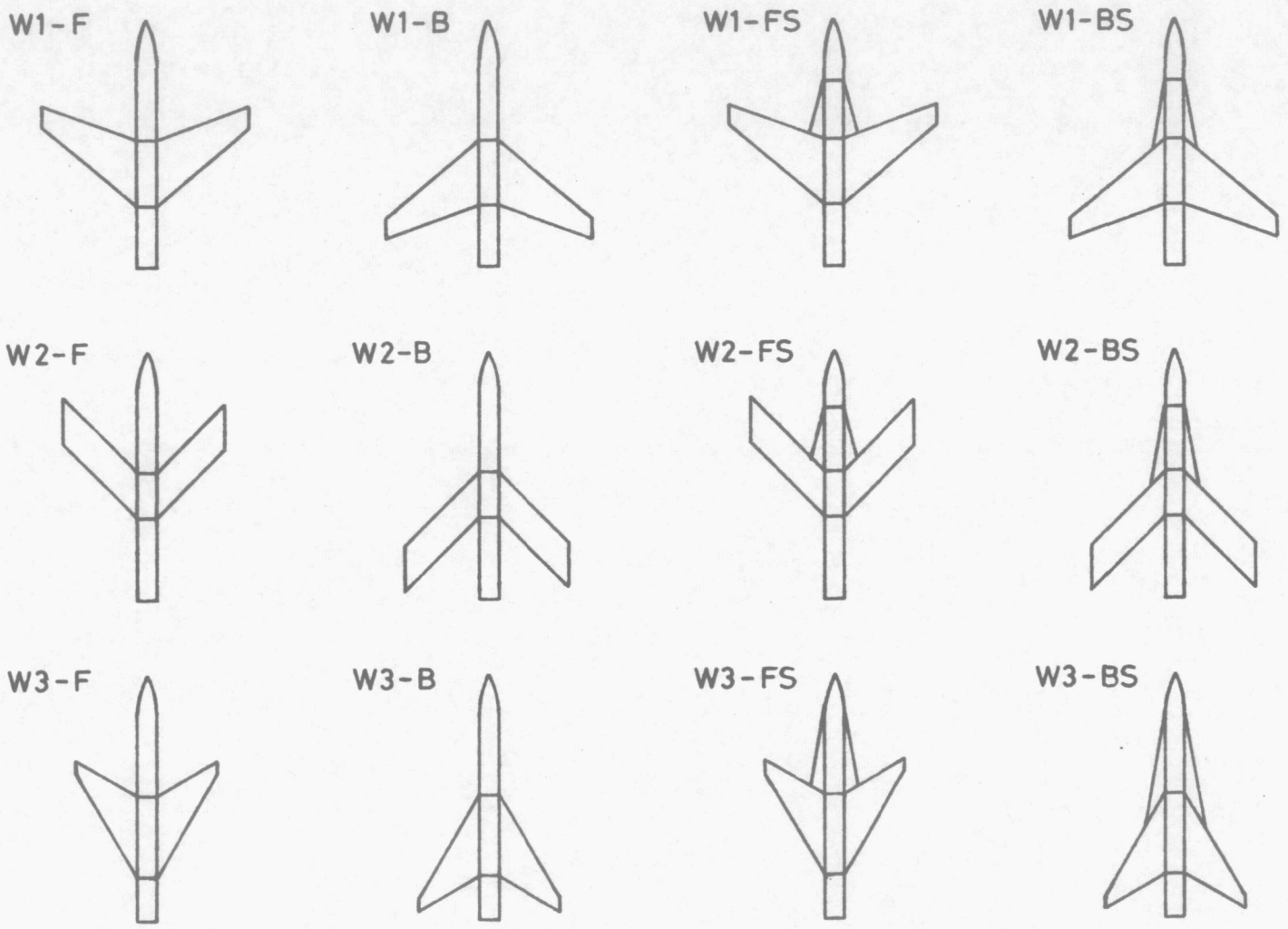

Figure 2. The wing / body and wing / body / strake configurations tested.

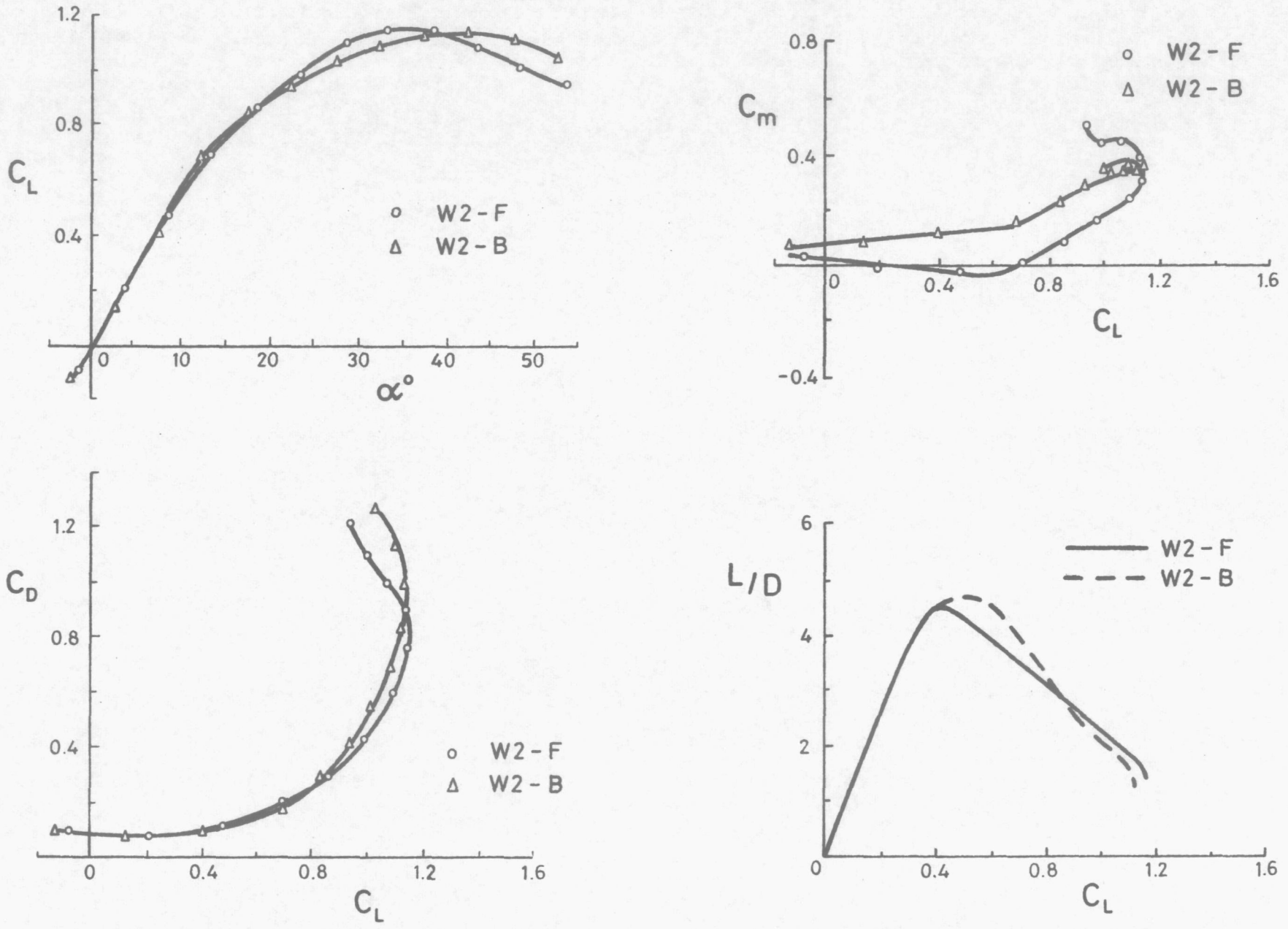

Figure 3. Force and moment measurements for planform W2.

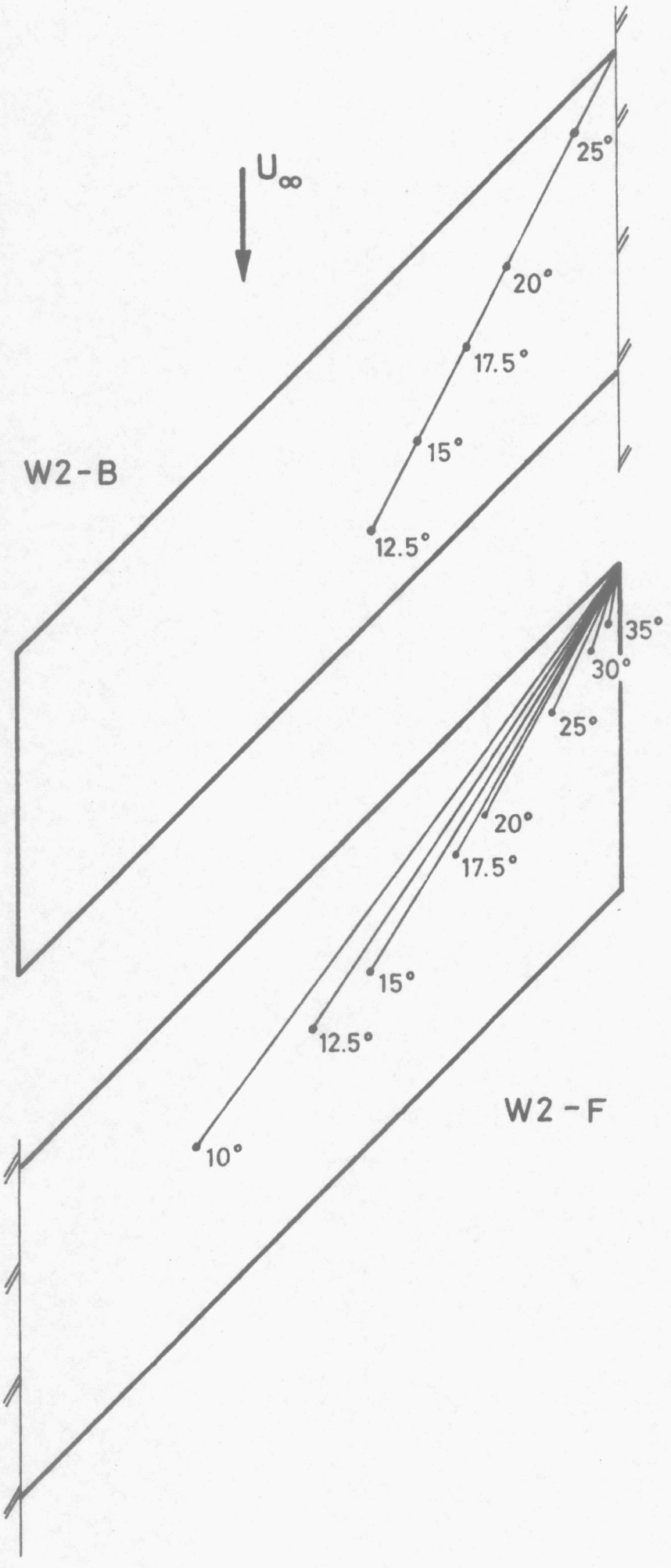

Figure 4. Orientation of vortex and location of vortex burst for planform W2.

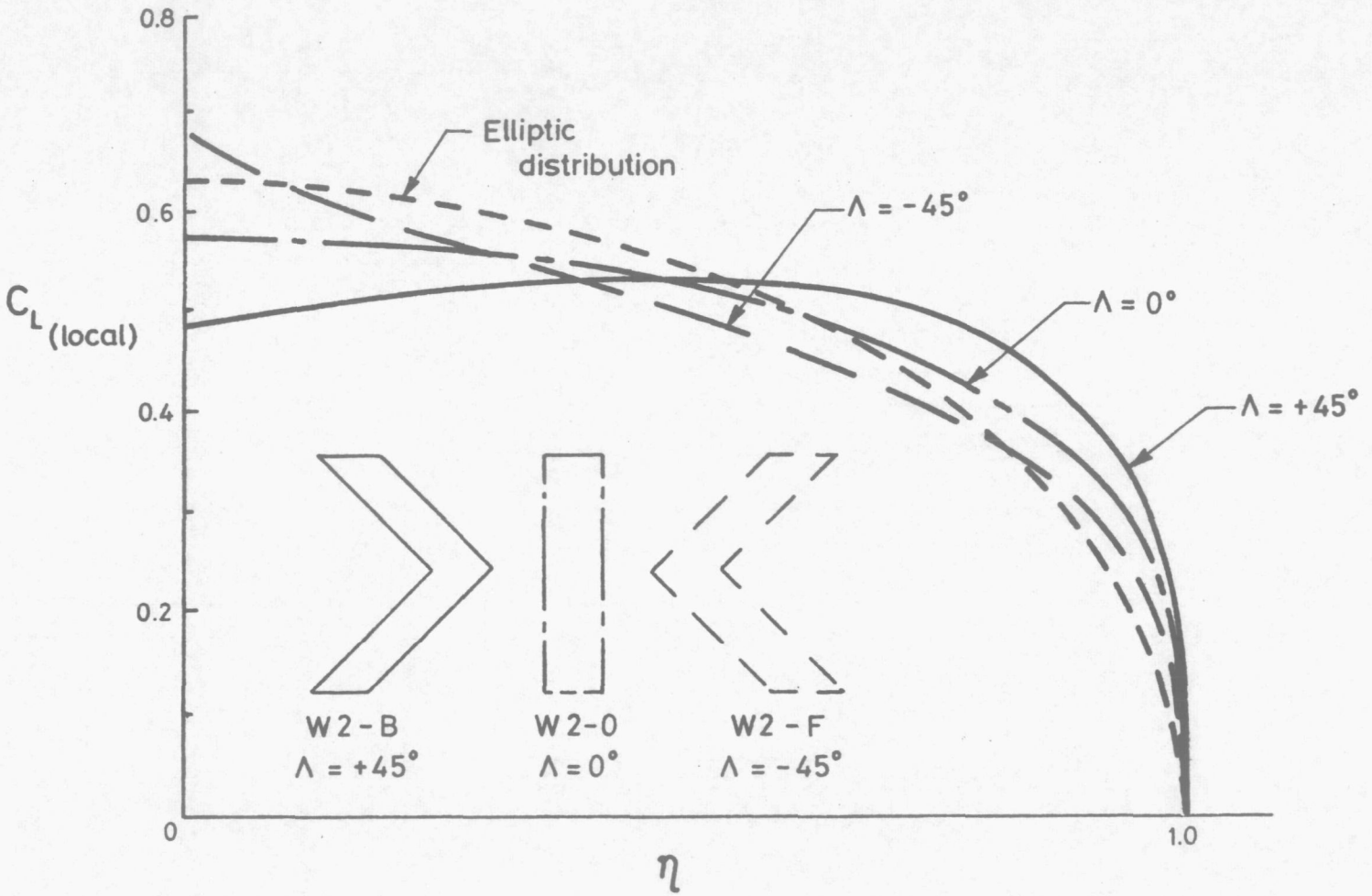

Figure 5. Spanwise lift distribution at C_L=0.5 as predicted by potential flow theory.

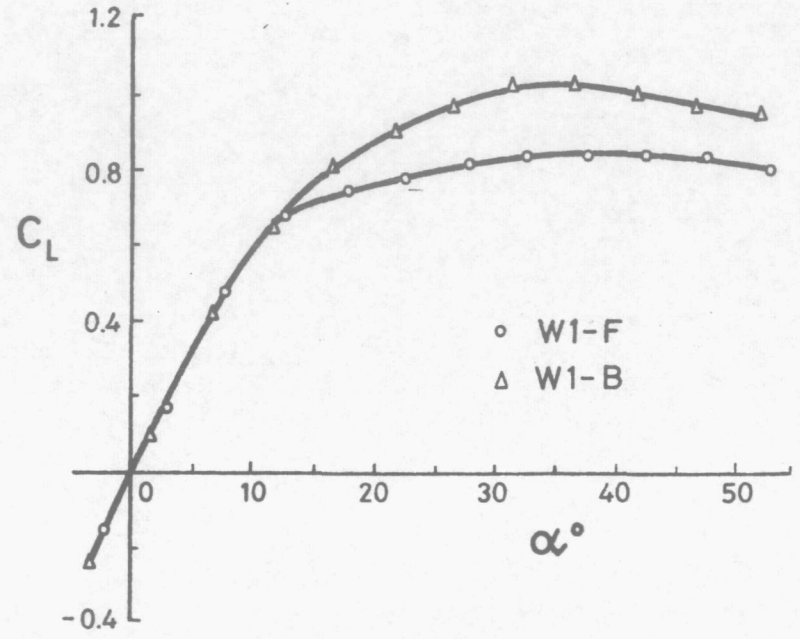

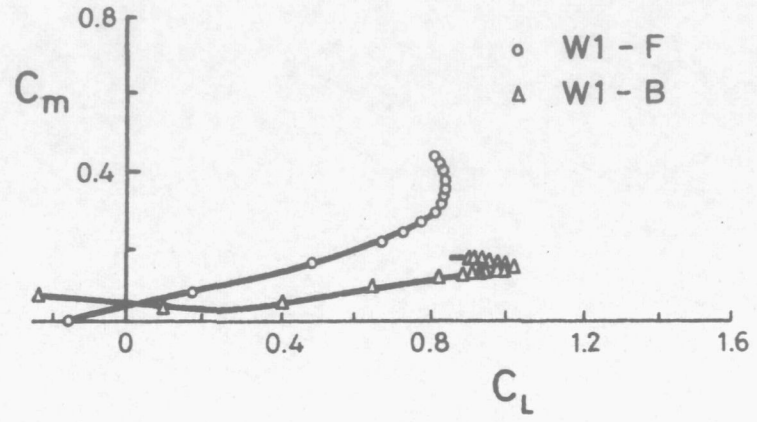

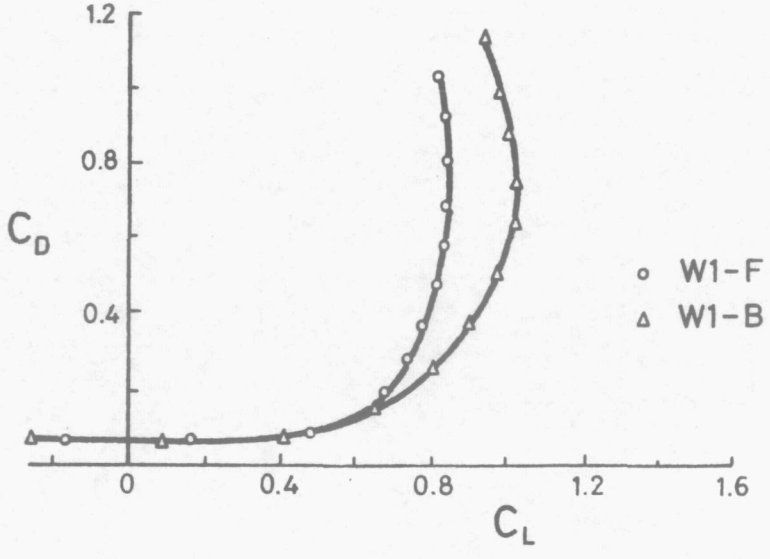

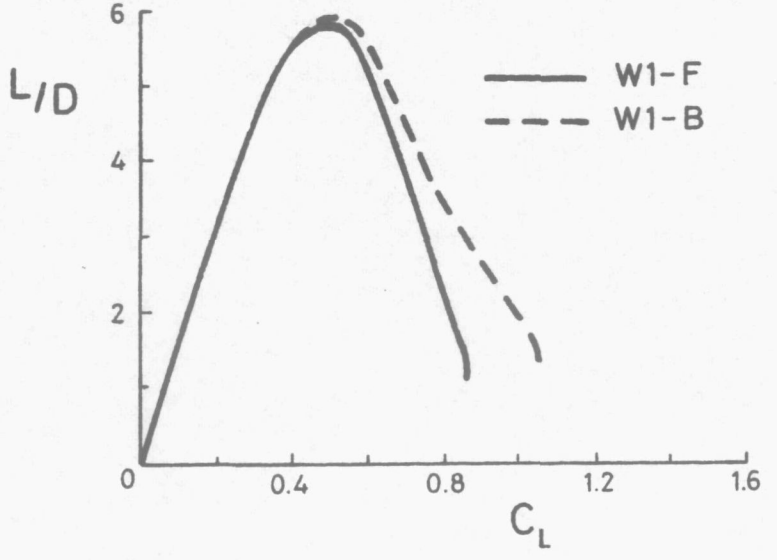

Figure 6. Force and moment measurements for planform W1.

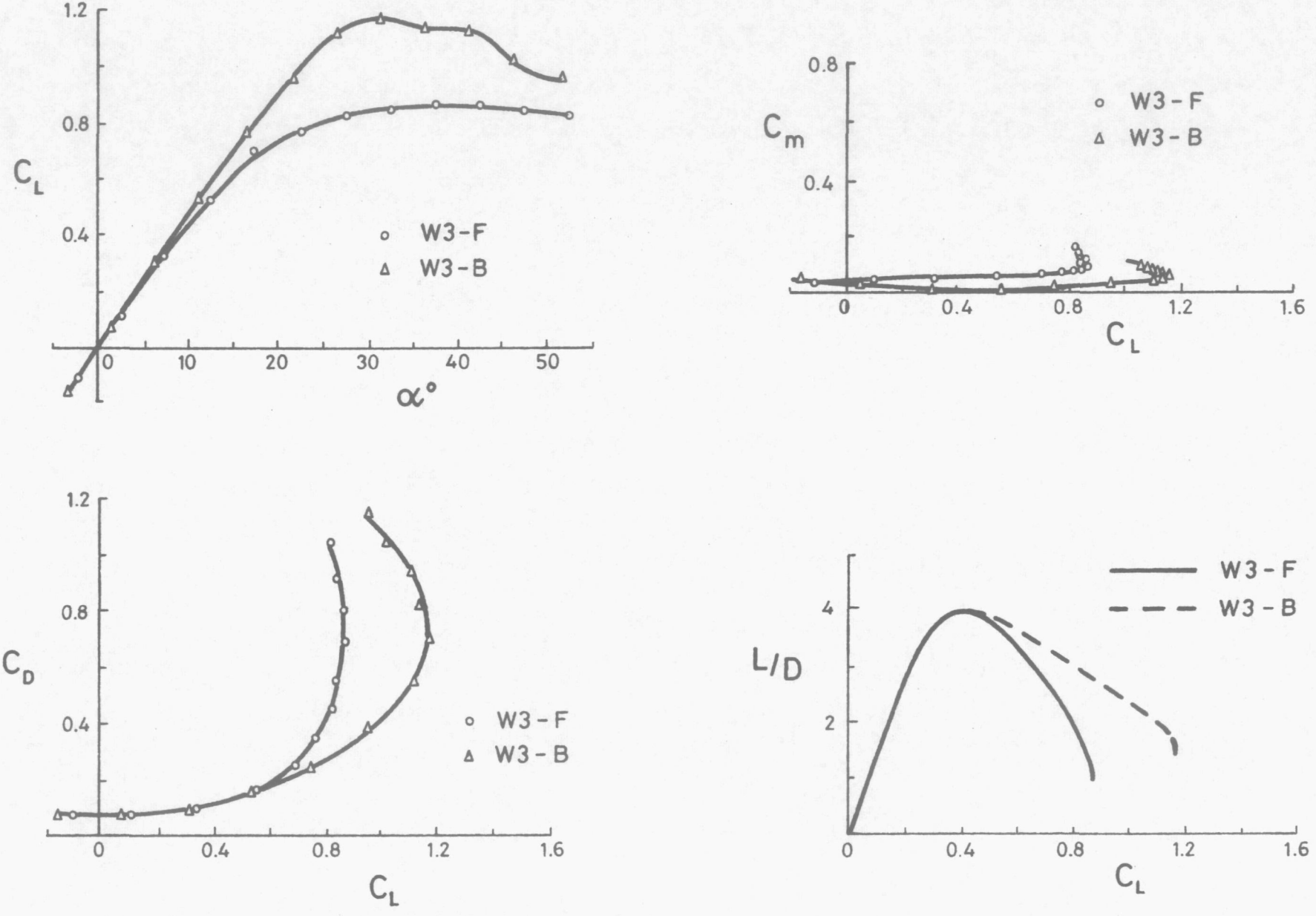

Figure 7. Force and moment measurements for planform W3.

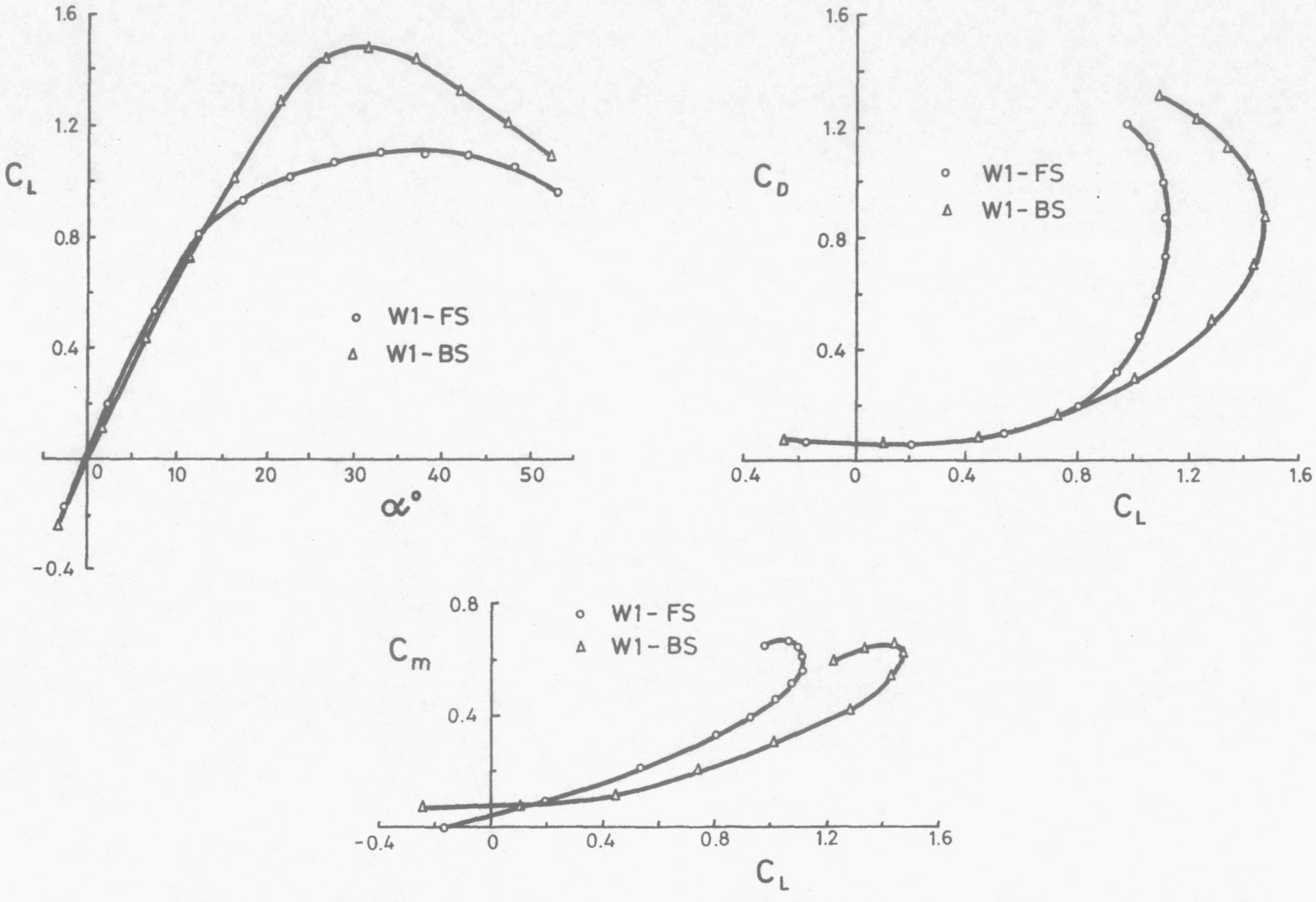

Figure 8. Force and moment measurements for planform W1-S.

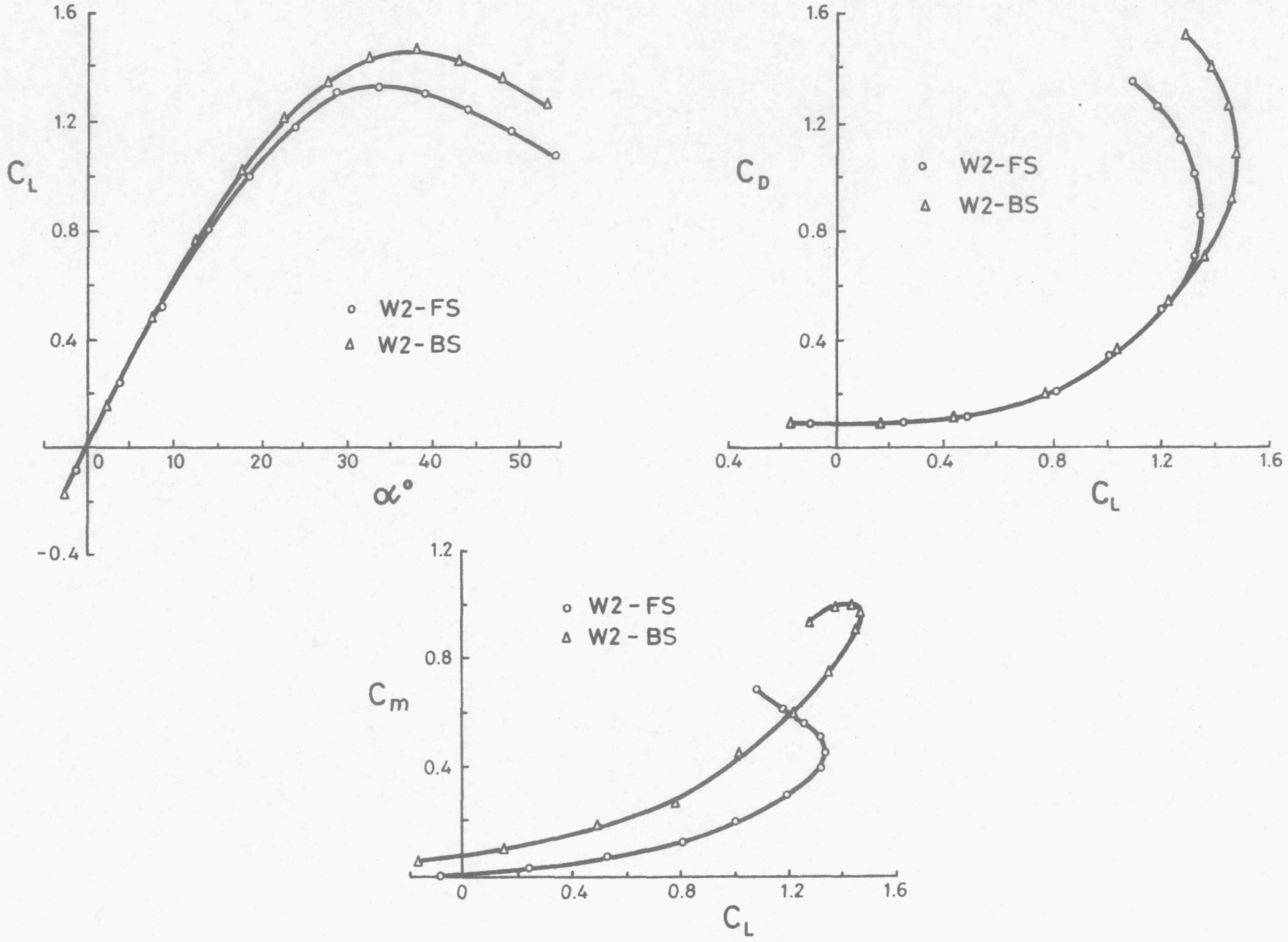

Figure 9. Force and moment measurements for planform W2-S.

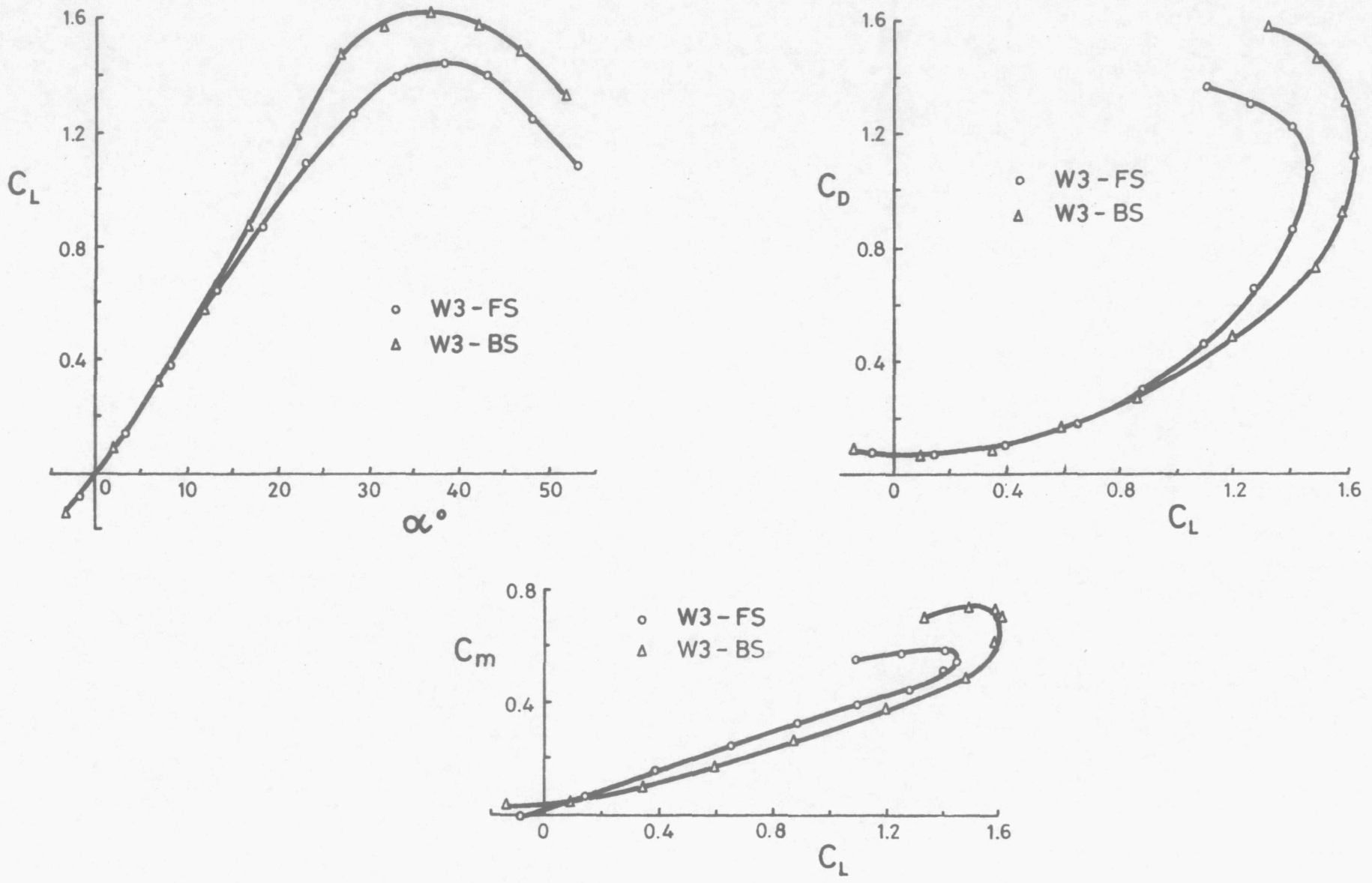

Figure 10. Force and moment measurements for planform W3-S .

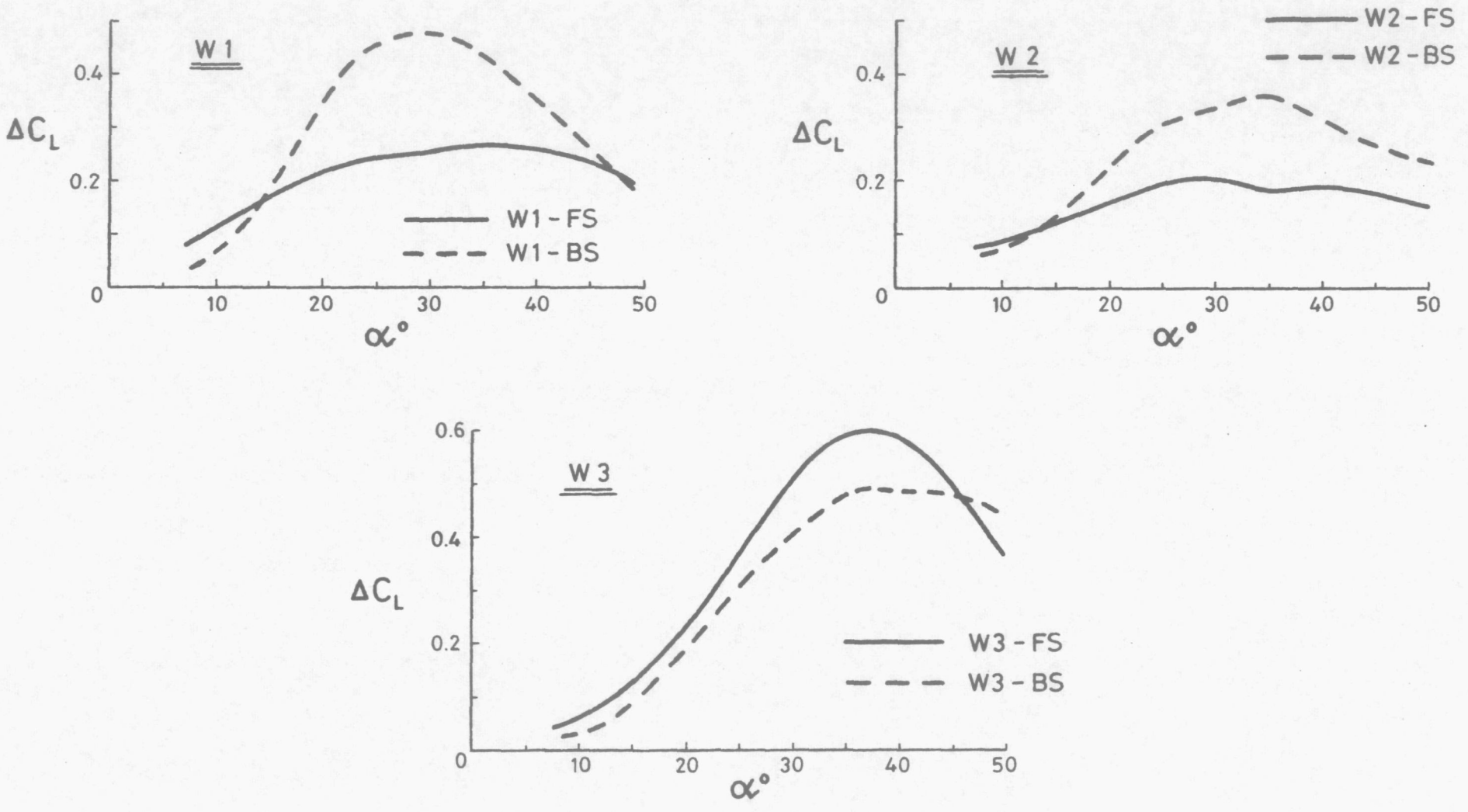

Figure 11. The variation of strake lift increment with incidence.

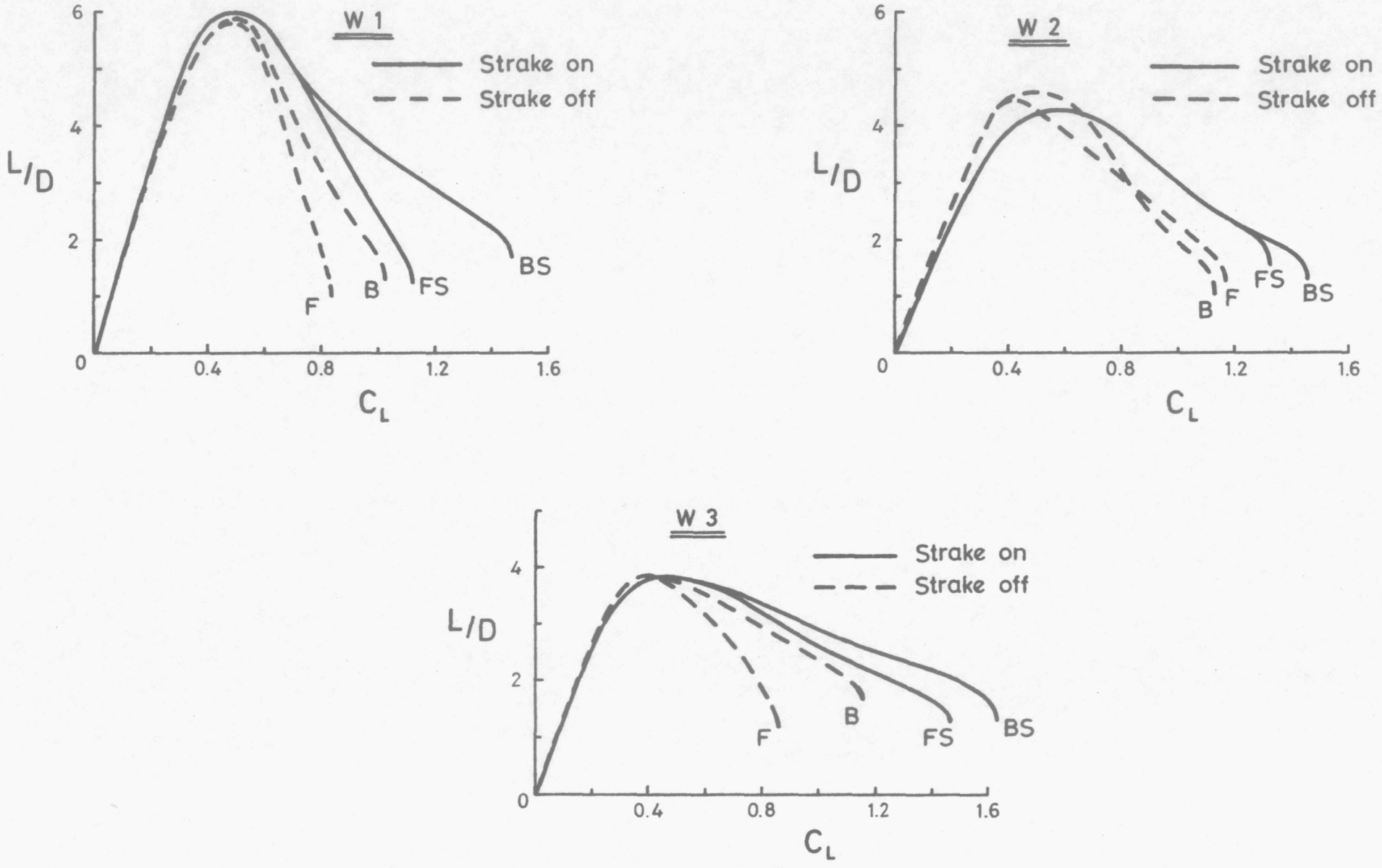

Figure 12. The variation of lift / drag ratio with lift coefficient.

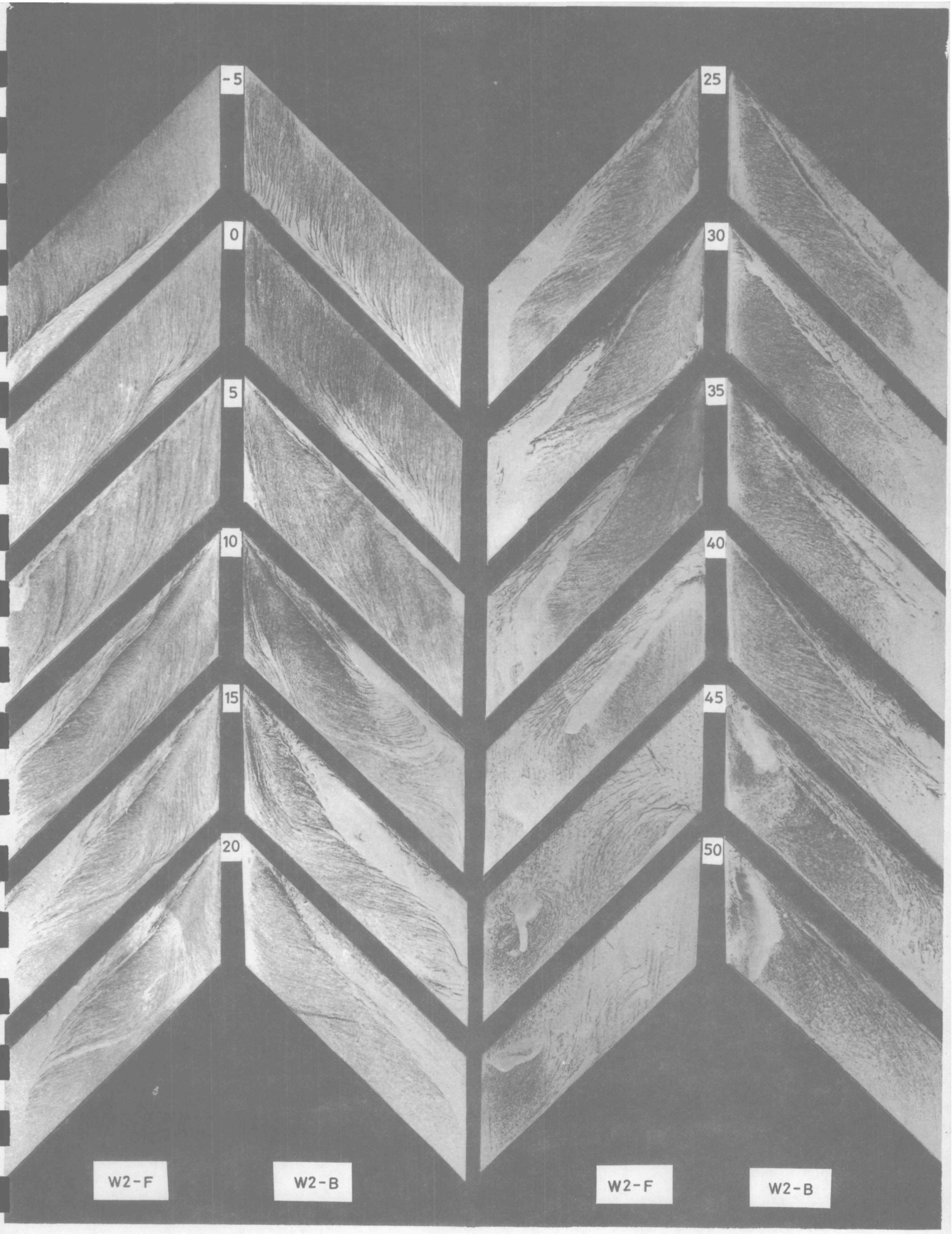

Plate 1. Surface oil-flow visualisations for planform W2.

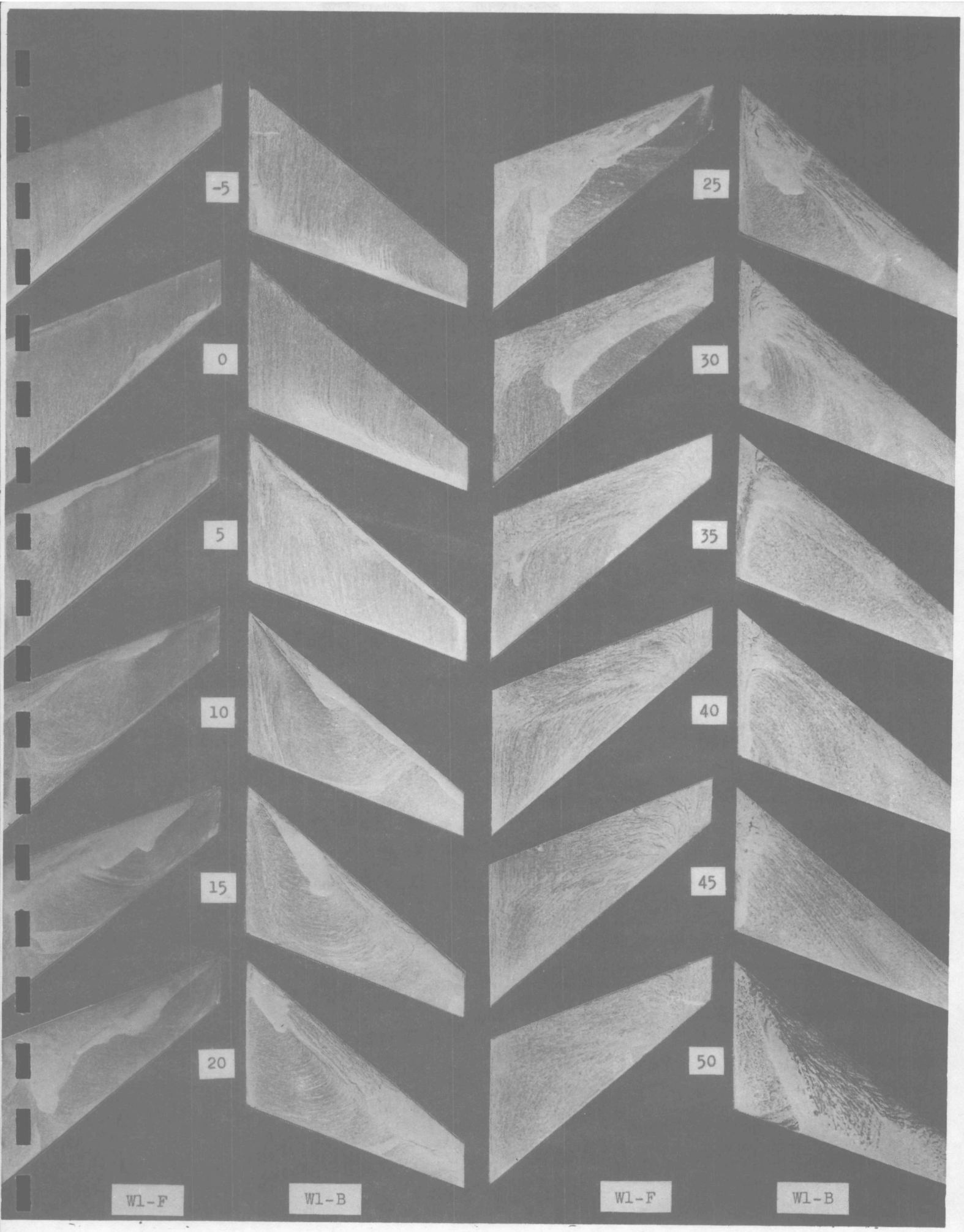

Plate 2. Surface oil-flow visualisations for planform W1.

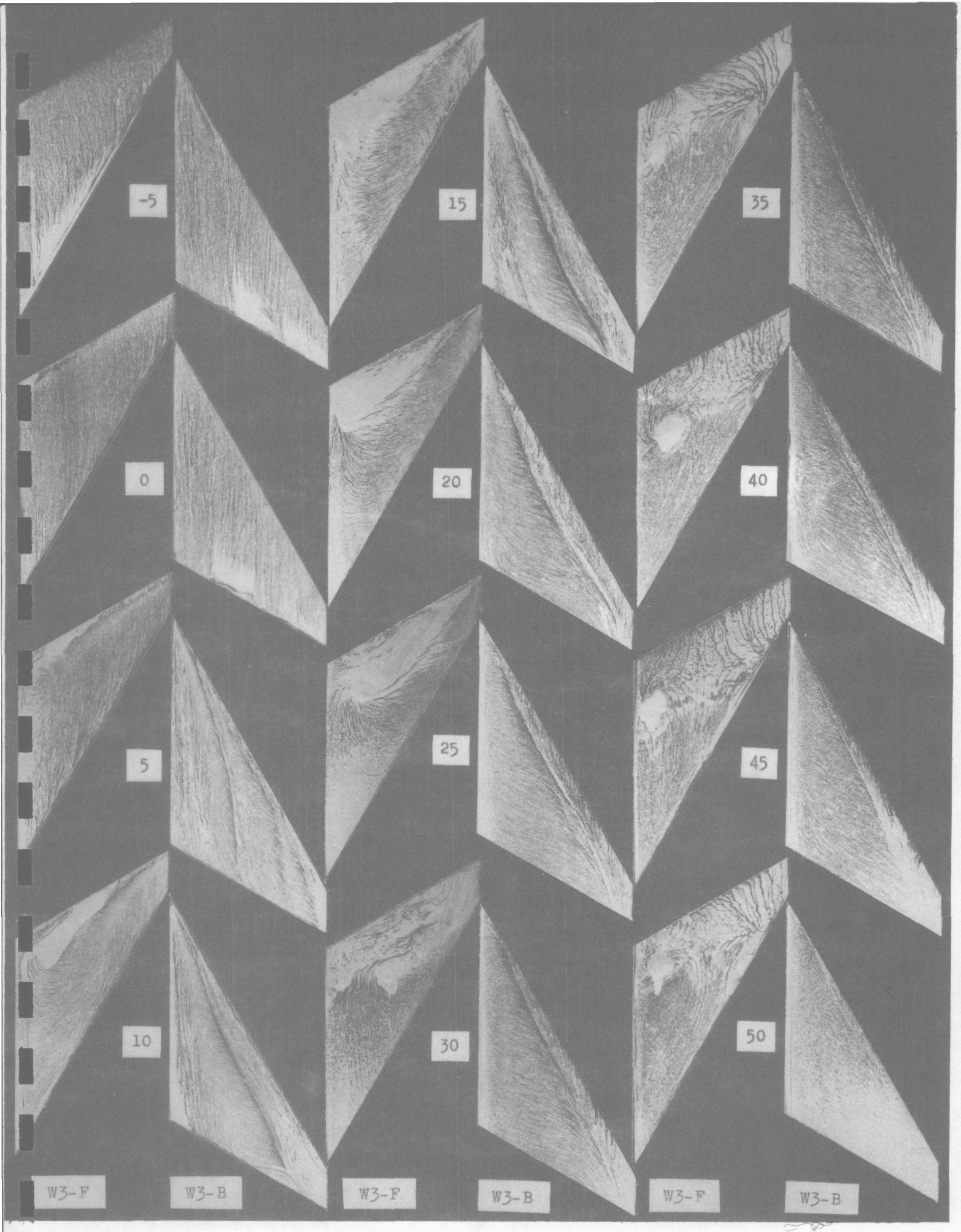

Plate 3. Surface oil-flow visualisations for planform W3.

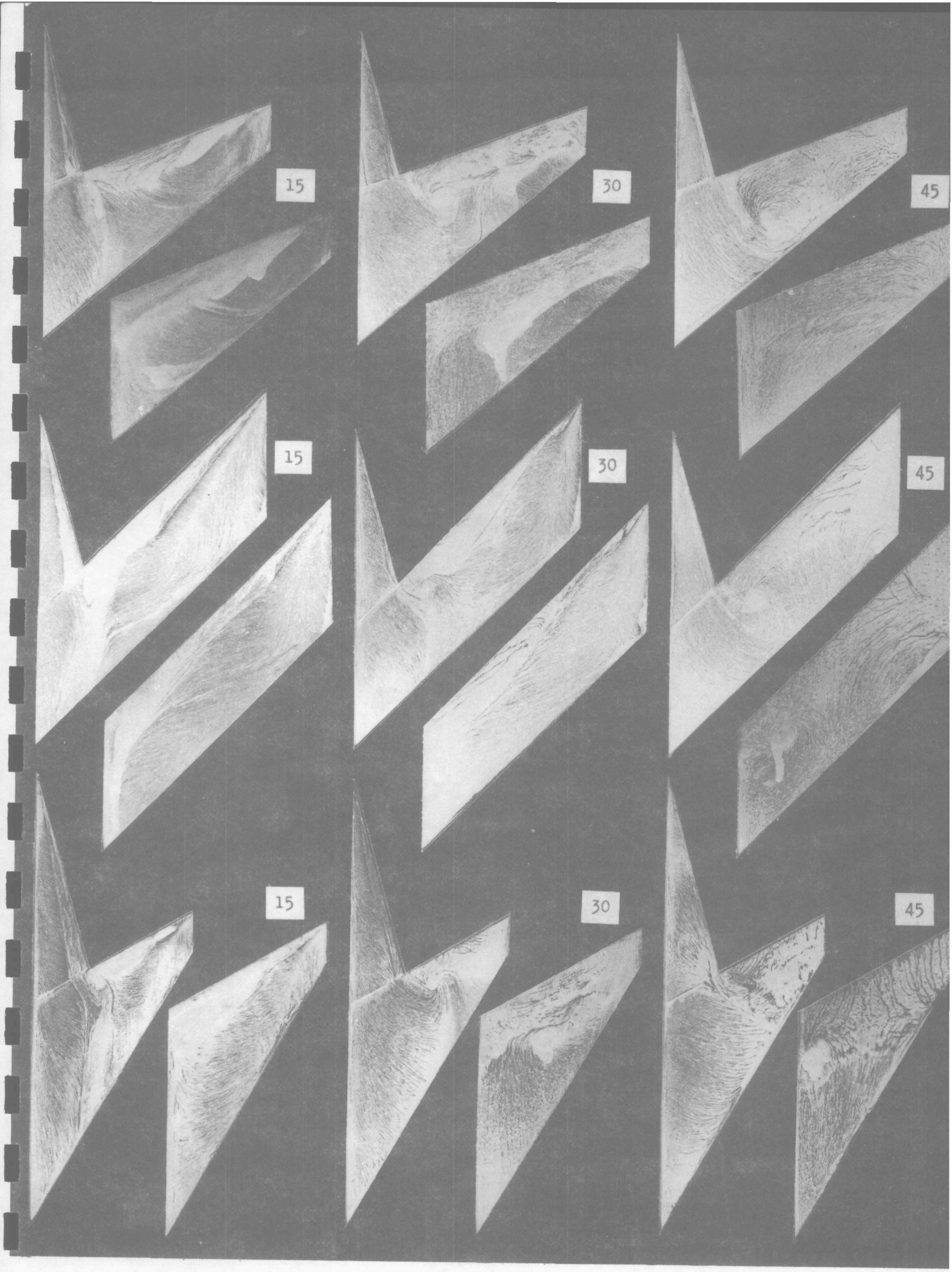

Plate 4. Surface oil-flow visualisations showing the effect of strakes upon the forward-swept configurations.

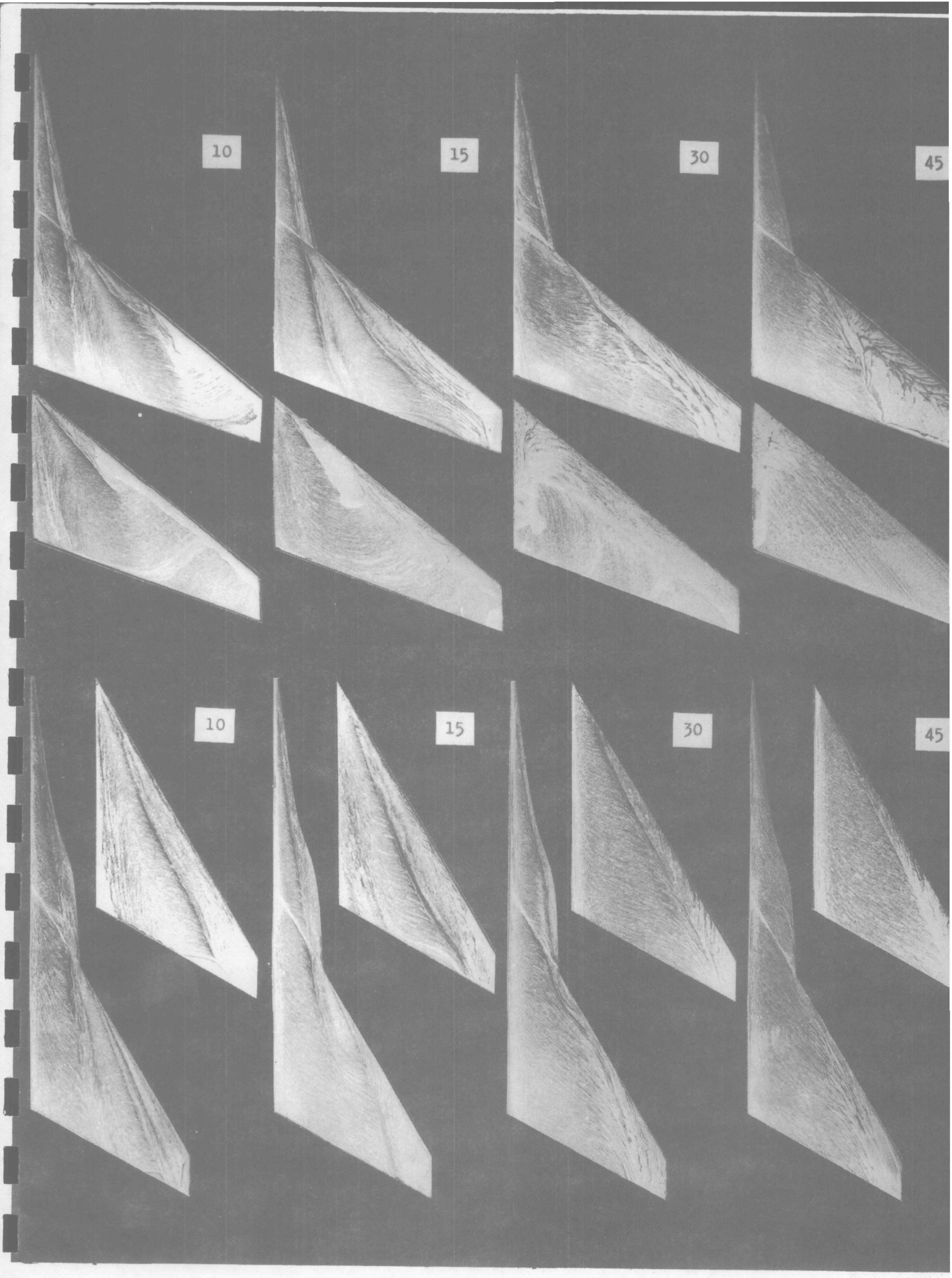

Plate 5. Surface oil-flow visualisations showing the effect of strakes upon the backward-swept configurations